Journal of Materials Chemistry B

Accepted Manuscript

ROYAL SOCIETY OF CHEMISTRY

www.rsc.org/materialsB

Bioactivated Protein-Based Porous Microcarriers for Tissue Engineering Applications

Baiwen Luo[1], Qiu Li Loh[1,2], Marcus Thien Chong Wong[3], Nguan Soon Tan[2,4], Cleo Choong[1*]

[1]School of Materials Science and Engineering, Nanyang Technological University, 50 Nanyang Avenue, 639798 (Singapore)

[2] Institute of Molecular and Cell Biology, Agency for Science, Technology and Research, 61 Biopolis Drive, Proteos, 138673 (Singapore).

[3] Department of General Surgery, Plastic, Reconstructive & Aesthetic Surgery, Tan Tock Seng Hospital, 11 Jalan Tan Tock Seng, 308433 (Singapore)

[4]School of Biological Sciences, Nanyang Technological University, 60 Nanyang Drive, 637551 (Singapore)

* Corresponding author:

Cleo Choong

Email: cleochoong@ntu.edu.sg

Tel: +65 6513 8166

Fax: +65 6790 9081Email: cleochoong@ntu.edu.sg

ABSTRACT

Microcarriers are commonly used in tissue engineering applications as they provide a large surface area for cell attachment. However, limited research has been done on ovalbumin (OVA), which is a relatively cheap protein found in avian egg white. Hence, in our current study OVA was fabricated into porous microcarriers and the effect of different OVA to alginate ratios on the properties of OVA microcarriers was investigated. Subsequently, in order to further improve cell-material interactions, extracellular matrix (ECM) material isolated from human lipoaspirate material was conjugated onto the porous OVA microcarriers using carbodiimide chemistry. A waste-to-resource strategy was employed to obtain this ECM material from human lipoaspirate material, which typically is discarded after surgery. This study illustrates the possibility of obtaining ECM material using a chemical-free decellularization method as well as the novel application of ECM material as a coating to confer bioactivity to protein-based microcarriers such as OVA. The incorporation of lipoaspirate-derived ECM (LpECM) into the OVA microstructure was shown to improve both mechanical strength and promote cellular growth on the microcarriers. The resulting porous OVA-LpECM hybrid microcarriers with tunable mechanical properties are examples of bioactivated porous protein-based microcarriers that can be applied to the field of tissue engineering.

INTRODUCTION

Currently, the most common treatment for various clinical problems such as severe burns and musculoskeletal disorders is the transplantation of tissue or organ.[1] However, the lack of suitable donor tissue or organs for transplantation typically results in a long waiting time for patients. Tissue engineering, which combines engineering and life sciences, is a promising approach to address this problem.[2] The most commonly used tissue engineering strategy is the incorporation of cells within a three-dimensional (3D) scaffold that mimics the native extracellular matrix (ECM) to regenerate or repair tissues.[3] The main challenge of this strategy is for sufficient numbers of cells of the desired phenotype to be obtained and delivered to the damaged site.[4] The conventional way of expanding cells has always been on a two dimensional (2D) platform, which requires multiple passages of monolayer cells to achieve the desired number. The multiple rounds of subculturing not only requires a long time for sufficient number of cells to grow, but there is also an inability to fully control and monitor the culture conditions throughout the subculturing process, which often leads to contamination in the long-term.[5] Hence, microcarriers that provide a high surface area for cell attachment has attracted great interest recently in tissue engineering applications.[5] Furthermore, the use of microcarriers as a 3D support matrix is more cost effective with regards to the amount of culture medium, cells, growth factors and space required for cell culturing. In addition, compared to normal 3D scaffolds, microcarriers can be injected directly into the body instead of being implanted using invasive surgical methods.[4,5]

Using this scaffold-based approach, successful tissue regeneration is greatly dependent on the biomaterial's properties.[6] Overall, the function of a biomaterial in tissue

engineering is to mimic the native scaffold, otherwise known as the ECM. The ECM plays an influential role in cell mitogenesis and chemotaxis, directs cellular differentiation, and is also able to induce constructive host tissue remodelling responses.[7] A number of materials, including poly(lactic acid),[8,9] alginate,[10] hydroxyapatite,[11] poly-lactic-co-glycolic acid,[12] gelatin,[13,14] and collagen[15] have been developed into microcarrier form. Interestingly, limited research has been carried out for ovalbumin (OVA), a relatively cheap protein mainly found in avian egg white. OVA is very similar to bovine serum albumin in terms of amino acid content and its genetic information is also similar to that of human serum albumin.[16] Recently, Yoo *et al*.[17] showed that albumin plays an important role in adipocyte differentiation by promoting lipid accumulation during adipogenesis, whilst Zoellner *et al*.[18] showed that serum albumin is a specific inhibitor of apoptosis in human endothelial cell. In addition, OVA was also reported to be used for bone application by Morgan *et al*.[19] and Supaphol *et al.*[20], as it was able to support the proliferation and differentiation of preosteoblast cells. Overall, OVA is easily available and also cheaper than the other natural polymers commonly used as scaffolding materials (e.g. collagen). Also, OVA has been shown to be biocompatible[19-21], and has the ability to degrade in the body into safe byproducts, unlike synthetic biodegradable polymers. However, the lack of cell adhesion receptors on the pure OVA material surface has greatly limited its applications in the field of tissue engineering.

As such, it is necessary to modify the OVA material surface in order to improve cell-material interactions. In our current study, we propose the use of ECM material isolated from discarded human lipoaspirate material, as a coating material for conferring

bioactivity to the OVA microcarriers. Previously, studies have shown that a variety of cellular events are regulated by the interaction between integrin receptors in the cell membranes and the ECM and that the ECM is able to induce constructive host tissue remodeling responses.[6,7] Hence, ECM as a material is highly instructive and can potentially be used as a tissue-specific coating material for enhancing the bioactivity of another material. Meanwhile, it has also been shown that adipose tissue is a rich source of ECM material.[3,7] However, to our knowledge, no study has yet been carried out to investigate the use of decellularized adipose tissue ECM directly as a coating material to improve bioactivity.

In the current study, a modified, inverse mould-leaching process was used to fabricate porous OVA microcarriers, which were subsequently coated with ECM material isolated from lipoaspirate waste. Overall, the present study investigates the effect of using different OVA to alginate ratios on the fabrication of porous microcarriers as well as the role of the ECM coating on the microcarriers' mechanical and biological properties.

MATERIAL AND METHODS

Materials

Freshly excised lipoaspirate samples were obtained from patients at Tan Tock Seng Hospital (TTSH), Singapore following procedures previously established by the National Healthcare Group Domain Specific Review Board (DSRB 2012/00071). All chemicals in the experiments were used as purchased and received from Sigma-Aldrich, Singapore unless otherwise stated.

Fabrication of OVA microcarriers

The OVA microcarriers were fabricated using an inverse mould-leaching method modified from Flynn *et al*.[3] The overall schematic for fabricating OVA microcarrier is shown in Fig. 1a. Briefly, 10% (w/w) OVA solution and 1% (w/w) alginate solution was prepared separately with different weight ratios (2:1, 1:1, 1:2) to obtain the OVA/alginate mixture. OVA/alginate microcarriers were fabricated using an electrostatic microcapsule generator (Nisco Var V1, Switzerland). The gelling bath consisted of 0.1 M calcium chloride that was constantly stirred with a magnetic stirrer to prevent microcarrier coalescence.[22] The crosslinking of OVA/alginate was allowed to proceed for 30 min at room temperature. Subsequently, the OVA/alginate microcarrier was transferred and soaked in 1% (w/w) 1,4-Butanediol diglycidyl ether (BDE) solution overnight at room temperature for complete crosslinking of OVA/alginate. The microcarriers were then washed using distilled (DI) water to remove the excess crosslinker before being immersed in 2% (w/w) sodium citrate bath under gentle shaking. The sodium citrate solution was changed every 10 min for three times to ensure complete removal of the

alginate at room temperature. Finally, OVA microcarriers were washed with DI water and freeze-dried.

Decellularization of lipoaspirate

In this study, the lipoaspirate ECM (LpECM) was isolated using a chemical-free method. Briefly, adipose tissue obtained by liposuction procedure, was rinsed with DIwater until all the blood components were completely removed. Subsequently, fresh DI water was added to the adipose tissue and homogenized at 15,000 rpm for 5 min. The tissue suspension was centrifuged at 5,500 rpm for 5 min and the upper lipid layer was discarded. Subsequently, the tissue suspension was washed by addition of DI water and placed into an ultrasonic cleaner for 5 min to help in the removal of cellular components. This 3-stage homogenize-centrifuge-ultrasonication process was repeated until a uniform suspension with no lipid layer was observed. Finally, the tissue suspension was placed into the freezer (-80ºC) overnight and freeze-dried for 24 h prior to use.

Characterization of LpECM

The isolated LpECM was fixed in 4% paraformaldehyde solution for 24 h, followed by rinsing in 1X phosphate buffered saline solution (PBS) before histological and immunohistochemical staining. All samples were paraffin-embedded and sectioned into 8 μm thick samples. Hematoxylin and eosin (H&E) staining was used to detect the presence of residual cells and cell nucleus, and to characterize the collagen structure of the LpECM. Briefly, the rehydrated sections were stained in hemotoxylin solution for 3 min, and differentiate in 0.1% hydrochloric acid solution for 2 s. Subsequently, the

sections were gently rinsed in running tap water for 3 min. Next, the sections were stained in eosin solution for 27 s and washed in DI water for 10 s. Finally the sections were mounted with glycerol and viewed under light microscope (Carl Zeiss Primo Vert, Germany).

Immunohistochemical staining was also used to localize human collagen type I, collagen type IV and laminin in the samples. The rehydrated sections were fixed with pure methanol and acetone at -20 ^{o}C for 10 min each. The sections were then blocked in a humid chamber with 0.1% Triton-X 100 and 2% bovine serum albumin (BSA) for 45 min at 25 ^{o}C. Subsequently, rabbit anti-human primary antibody against Collagen I, Collagen IV, and Laminin (Abcam, Singapore) diluted 1:100 in 2% BSA was added onto the sections respectively and incubated in a humid chamber overnight at 4 ^{o}C. Next, the sections were rinsed three times in 1X PBS for 5 min each. Goat anti-rabbit secondary antibody IgG (Abcam, Singapore) diluted 1:250 in 2% BSA was added and incubated in a humid chamber for 1 h at 4 ^{o}C. Finally, the sections were rinsed with 1X PBS and mounted using DAPI mounting medium. The presence of these structural proteins was observed under fluorescence microscope (Carl Zeiss Inc, Singapore).

The morphology of LpECM was investigated using the JEOL JSM-5410 (Japan) scanning electron microscope (SEM). Firstly, 2.5% glutaraldehyde solution was added to the LpECM and kept at 4 °C for 24 h. After fixation, the LpECM was rinsed with DI water and dehydrated using a graded ethanol series (30 min per change): 30%, 50%, 70%, 90%, 100% and 100%. The LpECM was then dried in 100% hexamethyldisilazane

(HMDS) for 10 min followed by air drying after HMDS was removed. After the LpECM was completely dried, it was placed onto carbon tape and coated with gold prior to imaging. An acceleration voltage of 5 x 10^3 V was used.

Preparation of lipoaspirate extracellular matrix (LpECM) coating material

Dried and milled LpECM was dissolved using 0.1 M HCl. The LpECM was allowed to digest for 48 h at 4 ºC under constant stirring. Finally, 0.1 M NaOH was slowly added to the LpECM solution in order to adjust the pH to 7.4. The LpECM solution was subsequently diluted to 1 mg/ml using 1×Dulbecco's phosphate buffered saline (DPBS, pH 7.4) solution (Life Technologies™, Singapore) prior to use.

Surface Modification of OVA microcarriers

LpECM was directly conjugated to the OVA-based microcarriers via carbodiimide chemistry, as shown schematically in Fig. 1b. The dried OVA-based microcarriers were first immersed in the LpECM solution, followed by the addition of 10 mg/ml of 1-ethyl-3-(3-dimethylaminopropyl)-carbodiimide (EDAC) and 2 mg/ml of N-hydroxysuccinimide (NHS) for the conjugation reaction. After 6 h, LpECM modified OVA microcarriers (OVA-LpECM) were washed with DI water and freeze-dried.

Microcarrier size and size distribution

100 random selected microcarriers were viewed under the light microscope (Carl Zeiss Primo Vert, Germany). The mean diameter and the distribution of microcarrier diameter were determined using the ImageJ software.

Fourier transform infrared (FTIR) spectroscopy

FTIR was used to detect the vibrations of chemical functional groups in the sample and to confirm both the successful crosslinking of the OVA microcarriers as well as the subsequent conjugation of LpECM material by detecting the presence of characteristic peaks. Briefly, the microcarriers were milled into fine powder and mixed with potassium bromide powder at a ratio of 1:20 and pelletized. Pure potassium bromide pellet was used as a reference. The absorption spectra were then collected and analysed using the Spectrum™ software.

Mechanical property

The compressive moduli of the microcarriers were determined using the Instron 5869 machine fitted with a 10 N load cell. Compression tests were carried out for five replicates of each type of sample at a crosshead speed of 0.01 mm/s until maximum extension was reached. The materials were tested in wet conditions, in which the microcarriers were submerged in saline for 24 h at 37ºC for complete wetting to take place. Next, Hertz analysis, which describes the linear elasticity of spheres compressed between two flat rigid surfaces for small deformations,[23] was carried out in order to correlate the compression force (F) with the displacement (H) as shown in equation (1):

$$F = \frac{4}{3}\sqrt{R}\left(\frac{E}{1-v^2}\right)\left(\frac{H}{2}\right)^{\frac{3}{2}} \qquad (1)$$

Where F refers to the force applied onto the microcarrier, R is the initial radius of the microcarrier, v refers to the Poisson's ratio, E the Young's modulus of the material and H the displacement. The Poisson's ratio was assumed to be 0.5 in this study.

Maximum swelling ratio

The stability of the microcarriers under physiological conditions (pH 7.4, 37^0C) was investigated by soaking the microcarriers in saline for 24 h to determine its maximum mass gained. The initial and final mass of the scaffolds was determined by a precision weighing balance (Fisher Scientific B-220C, Switzerland). The swelling ratio was determined using the following equation (2):

$$SW(\%) = \frac{M_f - M_i}{M_i} \times 100\% \qquad (2)$$

Where SW refers to swelling ratio, M_f is the final mass of microcarriers after 24 h soaking, and M_i is the initial mass of the microcarriers before the testing.

Cell viability test

StemPro® human adipose-derived mesenchymal stem cells (ASCs) were purchased from Life Technologies™, Singapore, and cultured using previously determined protocol[24]. Prior to cell seeding, 200 mg of ethylene oxide (EtO) sterilized microcarriers were weighed and placed into each well. 50 µL ASCs suspension was first seeded onto the microcarriers at a density of 10000 cells per well in a Poly (2-hydroxyethyl methacrylate) (Poly-HEMA) treated 24-well plate (Nunc). The additional 0.95 mL culture medium was added after 3 h. All the microcarriers were transferred to a new Poly-HEMA treated 24-well plate after 24 h, and the culture medium was changed every other day. The cell viability and proliferation of ASCs on the scaffolds was determined using the alamarBlue™ (AB) assay (Life Technologies™, Singapore) at 1, 3, 5 and 7 days time

points. At each time point, culture medium was removed from the wells, and the AB solution was added to the wells. The plates were incubated in a 5% CO_2 atmosphere at 37ºC for 4 h and the fluorescence density was measured using a microplate reader (Model 680, Bio-Rad Laboratories, Inc. Hercules, CA, USA) at an excitation wavelength of 570 nm and an emission wavelength of 580 nm. Cell numbers were calculated by seeding known quantities of cells and correlating them with fluorescence emission. The viability of cells in the 3D porous microcarriers was studied using LIVE/DEAD® viability/cytotoxicity assay. Briefly, 2mM Ethidium homodimer-1 and 4 mM Calcein AM dye were added to cell culture medium (1:1000 ratio) to produce a LIVE/DEAD® working solution. The cell-seeded microcarriers (after day 1 and day 7) were rinsed three times with PBS prior to staining with 0.5 ml of LIVE/DEAD® working solution. After incubation at 37ºC for 30 min in a 5% CO_2 atmosphere, the samples were imaged using a fluorescence microscope (Nikon Instruments, Tokyo, Japan) equiped with the NIS-Elements Br image software.

Statistical analysis

All tests were carried out in triplicates (i.e. n=3) with data shown as mean ± standard deviation unless otherwise stated. Analysis was carried out using two-way analysis of variance (ANOVA) with replicates. Data are considered to be statistically significant with a confidence level of 95% ($p<0.05$).

RESULTS

Characterization of LpECM

The whole decellularization process, which was used to process the lipoaspirate material, was completed under 2 h. As compared to current chemical and hybrid methods that often take days, the current decellularization process required a significantly shorter time.[7,25-27] Confirmation of decellularization was carried out using H&E staining, Picogreen® assay, immunostaining and scanning electron microscope (SEM). H&E staining results (Fig. 2a) showed no evidence of visible nuclear material, whilst the amount of dsDNA left in the dry LpECM was 49.3 ng/mg, which is within the limit stipulated for the clinical application of decellularized material.[7] SEM analysis further confirmed the removal of both cells and lipids (Fig. 2b) from the remaining fibrous LpECM material. Hence, in spite of the shortened processing time and the chemical-free approach, the LpECM achieved all the benchmarks of a successfully decellularized material.[7] Also, a change in colour from yellow to white was observed for the final freeze-dried LpECM (Fig. 2c). After freeze-drying, immunostaining results showed that key proteins such as collagen type I, collagen type IV and laminin remained intact in the LpECM (Fig. 2d-f).

Confirmation of crosslinking

FTIR was used to confirm the successful crosslinking of LpECM to OVA by the presence of characteristic peaks in the spectrum. Fig. 3 showed the FTIR spectra of raw OVA powder, OVA microcarrier and LpECM-modified OVA microcarrier. The strong peak

appearing at 3293 cm^{-1} was due to the functional group N-H stretching of amide A and amine within the OVA structure. The shallower band at 2961 cm^{-1} was linked to the asymmetrical stretch of $-CH_2$ for amide B. Besides amide A and amide B, another strong region was located in the range of 1000-1700 cm^{-1}: strongest peak for amide I at 1649 cm^{-1}, amide II at about 1535 cm^{-1}, and amide III caused two peaks around 1212 cm^{-1} and 1238 cm^{-1}. The strongest band of OVA, amide I, was almost entirely due to amide carboxyl C=O backbone stretching with a little effect from C-N stretching.[28,29] The combination of the N-H in-plane bend and the C-N stretching vibration made the amide II peak.[28] The peak of amide III peptide bond of OVA was generally responsible for a complex intermolecular interaction of OVA mainly from the C-N stretches and the N-H bending vibrations of peptide groups.[30] The observation of the peak at 1450 cm^{-1}, indicated that the α-helical secondary structure only exists in OVA powder.[31] The main difference between OVA powder and OVA microcarrier was the absence of amide II and amide III peaks and the appearance of two strong peaks at 1408 cm^{-1} and 1029 cm^{-1}. Another minor difference was the decrease of the peak intensity at 3271 cm^{-1}. These can be explained by the successful crosslinking of OVA and BDE (Fig. 4). Due to the reaction of free amine groups ($-NH_2$) of OVA and epoxide groups at the two ends of BDE, more hydroxyl functional groups and C-N bonds were formed with the further consumption of amine and amide groups. As such, a reduction in the characteristic peak of amide A and the disappearance of amide II was observed. The peak at 1408 cm^{-1} was mainly due to the O-H in-plane bending and the one at 1029 cm^{-1} was due to the C-N stretching and the C-O stretching from alcohol. The loss of amide III might be caused by the breaking down of the secondary structure of OVA during the reaction. With the

LpECM modified microcarriers, the amide III peak re-appeared in the spectrum, which was due to the introduction of the complex mixture of proteins within LpECM. The additional peak at 1704 cm^{-1} was due to the C=O stretching of carboxylic group within the LpECM proteins. The appearance of amide I at a lower region was also observed. This was because the OVA microcarrier was further crosslinked by EDAC/NHS during the modification step.

Morphology

As the result of BDE crosslinking, the mean diameter of OVA microcarriers was 908 ± 62 μm (Fig. 5a) and the size distribution indicated that 74% of OVA microcarriers (n=100) ranged between 850-950 μm. After modification with LpECM, the average size, and size distribution of microcarriers have no significant differences (Fig. 5e and 5i). An interconnected network of random-sized pores could be observed under the SEM (Fig.5b-d for OVA microcarriers and Fig. 5f-h for OVA-LpECM microcarriers). With the aid of ImageJ software, the pore size range and porosity of scaffolds was determined (Table 1). With an increase in alginate proportion, the porosity of resulting OVA microcarriers increased from 33.7% for 2:1 (OVA : alginate) weight ratio to 57.4% for 1:2 (OVA : alginate). After LpECM coupling, the porosity was reduced slightly for all the microcarrier groups. In addition, there was no significant difference of the mean pore size and pore size range of OVA and OVA-LpECM microcarriers with different OVA to alginate ratios.

Mechanical testing

Compression testing was carried out until 40% strain was reached. Both OVA and OVA-LpECM microcarriers were observed to recover within a short period of time (i.e. ~15s). However, increasing the proportion of alginate for the microcarriers led to a decrease in compressive modulus for both the OVA and OVA-LpECM microcarriers (Fig. 6). Also, when compared to the pure OVA microcarriers, the OVA-LpECM microcarriers with the same corresponding OVA to alginate ratio exhibited significantly improved mechanical strength.

Swelling ratio

In order to simulate the conditions that the microcarriers will be subjected to in a clinical setting, the microcarriers were left in saline and the water absorbing capacity of the different groups of microcarriers was determined by their swelling ratios. It was found that with increasing alginate content, the swelling ratio for the microcarriers also increased, except for the case of 1:1 (OVA : alginate) OVA microcarrier (Fig. 7).

Cell Proliferation

The efficacy of OVA and OVA-LpECM microcarriers for supporting the growth and proliferation of ASCs was evaluated in this study. There is no significant difference on cell study results for microcarriers with the different OVA to alginate ratios. Therefore, the cell study results of the microcarriers with OVA to alginate ratio of 1:1 were shown in Fig 8. The initial cell attachment was significantly increased ($*p<0.05$) after the pure OVA microcarrier was modified with LpECM. In addition, after a culture period of 7 days, almost twice the number of cells was observed on the OVA-LpECM microcarriers

as compared to the pure OVA microcarriers (Fig. 8). The LIVE/DEAD staining of ASCs after 1 day and 7 days culture on OVA and OVA-LpECM microcarriers was shown in Fig. 8b-e. OVA-LpECM microcarriers showed much better cell attachment and proliferation. For OVA microcarriers, the attached ASCs appeared to have a more rounded cell morphology, as compared to the ASCs on LpECM modified OVA microcarrier. Hence, our current results showed that the addition of LpECM to the OVA microcarriers significantly improved (*p<0.05) the cell-material interactions, resulting in an enhanced cell proliferation profile for the LpECM-containing microcarriers.

DISCUSSION

A purely physical decellularization method involving multiple cycles of centrifugation, homogenization, and ultrasonication in order to remove all cellular and lipid components from the original adipose tissue, was successfully developed to obtain LpECM material. Overall, the whole decellularization process used to treat the lipoaspirate material took place in just 2 h as compared to current chemical and hybrid methods that often take days.[7,25-27] Also, our current method allowed for the processing of lipoaspirate material without involving any harsh chemicals, thereby allowing for a better potential for clinical translation to the surgical theatre. It is noted that with current methods, the chemicals required for the decellularization process may cause damage not only to the ECM material itself, but also increase the possibility of immune rejection as they are often present in the final ECM material used, even after repeated rinsing.[7] Overall, despite the shortened processing time and the chemical-free approach, the LpECM achieved all the benchmarks[7] of a successfully decellularized material as shown in Fig. 2.

Preservation of ECM composition is highly desirable in tissue decellularization process as there is a fine balance between effective decellularization and the removal of key proteins that contribute to the bioactivity of the ECM. From the immunostaining results, key ECM proteins such as collagen type I, collagen type IV and laminin remained intact in the LpECM. In fact, even after freeze drying, which allows for long-term storage of the LpECM material and hence off-the shelf availability for the surgeon, the same key ECM proteins were preserved. This dry form of LpECM also allows for easier storage and transportation, thus allowing for greater possibility for scale-up and commercialization in the long-term.

For this study, the decellularized LpECM was subsequently used as a material for conjugation to OVA to confer additional bioactivity to the microcarriers. FTIR results confirmed successful crosslinking of OVA solution to form OVA microcarriers and the coupling of LpECM to OVA microcarriers from the characteristic peaks.

The morphologies of the OVA and OVA-LpECM microcarriers were examined under the SEM and interconnected pores (Fig. 5) of random sizes (Table 1) were observed for all groups. In general, the porosity and pore size of the OVA microcarriers were shown to be tunable by altering the amount of alginate (Table 1), since the alginate acts as a porogen during the inverse moulding process. Thus, with the increase in alginate content, the porosity of the microcarriers also increased. As such, 1:2 (OVA : alginate) microcarriers had significantly higher porosity than 2:1 (OVA : alginate) microcarriers. The porosity of the OVA-LpECM microcarriers was slightly reduced after LpECM coupling due to two main reasons. The first reason is that after the modification process, LpECM material was coated on all the surfaces of the pore structure, which consequently led to a decrease in the overall pore volume. The other reason, as seen from the decrease in amide A peak after LpECM modification (Fig. 3), is due to the strengthening of the microcarriers and reduction in porosity after LpECM modification as the result of the OVA reaction with EDAC/NHS itself during the modification process. In general, the porosity of the microcarriers plays an important role in affecting cell proliferation, migration, and vascularization.[32]

During the compression testing, both OVA and OVA-LpECM microcarriers were observed to be able to recover their shapes within seconds. This suggests that the microcarriers had a shape memory effect as they quickly recovered their spherical shapes

after mechanical deformation. This property would be useful when injecting the microcarriers to specific sites *in vivo*, since these microcarriers can be compacted into a small fraction of their original size.[33] With the increase in alginate to OVA ratio, a decrease in compressive moduli was observed for both OVA and OVA-LpECM microcarriers (Fig. 6). As seen from the microcarrier fabrication process (Fig. 1), alginate acts as a sacrificial material, which is why a higher amount of alginate would lead to increased porosity in the resulting OVA material. Also, the conjugation of LpECM to OVA micrcarriers led to improved mechanical strength of the OVA-LpECM microcarriers as compared to uncoated OVA microcarriers since the additional crosslink happened during the coating process.

Another effect of increasing the alginate content of the microcarriers is that their swelling ratio also increases. The only exception was the OVA microcarrier with OVA to alginate ratio of 1:1, which did not have a significant change in swelling ratio compared to the OVA microcarrier with OVA to alginate ratio of 2:1. This may be the result of a balance between the OVA content and total porosity caused by the removal of alginate. In general, the increase in the swelling ratio was probably due to the increase in porosity with increasing alginate content, which enabled more fluid to be absorbed into the microcarrier. However, after the LpECM modification, the swelling ratio was shown to decrease for the two groups with OVA : alginate ratios 2:1 and 1:1, and increase for one group of OVA : alginate ratio 1:2 (Fig. 7). This phenomenon could be due to the balance between the decrease of the porosity after the modification (Table 1) and the introduction of more hydrophilic groups from the LpECM material. Due to higher surface area caused by higher porosity, there was more area for LpECM to be coated on. Therefore, the only

group with increasing swelling ratio after LpECM modification was the group from highest porosity originally (OVA : alginate ratio 1:2). Swelling capability affects the *in vivo* stability of the microcarriers. In general, swelling plays important role in diffusion and transportation to maintain the viability of cells. A high swelling ratio will ultimately reduce the stability of the microcarriers during application,[13,14] but will facilitate cell seeding onto the microcarriers as greater porosity will be present.[14] Hence, a an ideal cell carrier material will have the right balance between the two properties.

The efficacy of the uncoated OVA and OVA-LpECM microcarriers to support the proliferation and growth of ASCs was also shown to be significantly different (Fig. 8). As LpECM was directly derived from adipose tissue, it retained various biological components from original native microenvironment (Fig. 2). Thus, more cells were attached onto the OVA-LpECM microcarriers due to the incorporation of cell adhesion receptors from LpECM to OVA, and a higher cell proliferation rate was also observed for the LpECM-enriched OVA microcarriers. Overall, the enrichment of OVA with ECM addresses the lack of cell adhesion receptors on OVA, which is one of the main challenge when using OVA for tissue engineering applications[34]. In this study, the efficacy of the porous microcarriers is largely dependent on the surface property, rather than the porosity and pore size. In previous studies within our group, we also showed that other natural and synthetic polymers, including alginate and polycaprolactone (PCL), could be successfully modified using the same conjugation method used in this study (Supplementary Fig. S1). Overall, LpECM-coating of microcarriers led to improvements in cell-material interactions and facilitated the cell growth and proliferation.

CONCLUSION

Porous OVA microcarriers were successfully fabricated by an inverse mold-leaching process. The alginate served as a sacrificial mold in this fabrication method because it can be rapid gelled by electrostatic crosslinking and easily removed in sodium citrate by the ion exchange process. Pore size and porosity can be tuned by modulating the OVA to alginate ratio used for fabricating the OVA microcarriers. In order to improve the bioactivity of the OVA material, ECM material was conjugated onto OVA, thus resulting in the development of novel hybrid microcarriers. In order to obtain the ECM material, a chemical-free decellularization method was developed to obtain LpECM from human lipoaspirate waste material within a short processing time. Key proteins such as collagen type I, collagen type IV and laminin, which are important for cell attachment and growth, were preserved in the LpECM. Thus, LpECM was used to enrich the OVA material, resulting in the formation of porous, bioactive OVA-LpECM microcarriers. The incorporation of LpECM into the OVA microstructure was also found to improve mechanical strength as well as promote growth and proliferation of ASCs. However, it should be pointed out that OVA, is just one of the materials that can be enriched with LpECM (i.e. a waste-to-resource biomaterial) to form eco-friendly hybrid biomaterials that could be potentially used for tissue engineering applications.

Overall, LpECM enrichment, using LpECM material that has been physically instead of chemically treated, was able to provide the necessary cell adhesion receptors and other essential biological factors for improving cell-material interactions. Taken together, these bioactivated protein-based microcarriers with tunable mechanical properties could potentially be used as injectable fillers for either soft tissue or bone tissue engineering applications.

Acknowledgments

The electron microscopy work was performed at the Facility for Analysis, Characterization, Testing and Simulation (FACTS) in Nanyang Technological University, Singapore.

This work was funded by Nanyang Technological University (NTU) and National Healthcare Group (NHG) innovation seed grant.

References

1. M.S. Chapekar, *J. Biomed. Mater. Res.,* 2000, **53,** 617-620.

2. R. Langer, *Tissue Eng.,* 2007, **13,** 1-2.

3. A.E.B. Turner and L.E. Flynn, *Tissue engineering Part C, Methods,* 2012, **18,** 186-197.

4. J. Malda and C.G. Frondoza, *Trends Biotechnol,* 2006, **24,** 299-304.

5. T.K.P. Goh, Z.Y. Zhang, A.K.L. Chen, S. Reuveny, M. Choolani, J.K.Y. Chan and S.K. Oh, *BioResearch Open Access*, 2013, **2,** 84-97.

6. H. Tan, L. Wan, J. Wu and C. Gao, *Colloids Surf. B Biointerfaces,* 2008, **67,** 210-215.

7. P.M. Crapo, T.W. Gilbert and S.F. Badylak, *Biomaterials*, 2011, **32,** 3233-3243.

8. X. Shi, L. Sun, J. Jiang, X. Zhang, W. Ding and Z. Gan, *Macromol. Biosci.*, 2009, **9,** 1211-1218.

9. Y. Hong, C. Gao, Y. Xie, Y. Gong and J. Shen, *Biomaterials*, 2005, **26,** 6305-6313.

10. C. Halberstadt, C. Austin, J. Rowley, C. Culberson, A. Loebsack, S. Wyatt, S. Coleman, L. Blacksten, K. Burg, D. Mooney and W.J. Holder, *Tissue Eng.*, 2002, **8,** 309-319.

11. L.Y. Sun, S.Z. Lin, Y.S. Li, H.J. Harn and T.W. Chiou, *Cell Transplant*, 2011, **20,** 49-62.

12. S.W. Kang, O. Jeon and B.S. Kim, *Tissue Eng.*, 2005, **11,** 438-447.

13. J.M. Melero-Martin, M.A. Dowling, M. Smith and M. Al-Rubeai, *Biomaterials*, 2006, **27,** 2970-2979.

14. J.Y. Lai, D.H.K. Ma, M.H. Lai, Y.T. Li, R.J. Chang and L.M. Chen, *PloS one*, 2013, DOI: 10.1371/journal.pone.0054058.

15. M. Overstreet, A. Sohrabi, A. Polotsky, D.S. Hungerford and C.G. Frondoza, *In Vitro Cell Dev. Biol. Anim.*, 2003, **39,** 228-234.

16. J.C. Lewis, N.S. Snell, D.J. Hirschmann and H. Fraenkel-Conrat, *J. Biol. Chem.*, 1950, **186,** 23-35.

17. W. Yoo, J. Lee, S. Park, Y.S. Kim, C. Lim, E. Yoon, G. Hur and J, Oh, *Biochem. Biophys. Res. Commun.*, 2010, **397,** 170-175.

18. H. Zoellner, M. Höfler, R. Beckmann, P. Hufnagl, E. Vanyek, E. Bielek, J. Wojta, A. Fabry, S. Lockie and B.R. Binder, *J. Cell Sci.*, 1996, **109,** 2571-2580.

19. G. Farrar, J. Barone and A. Morgan, *Journal of Tissue Engineering*, 2010, DOI: 10.4061/2010/209860.

20. P.R. K-hasuwan, N. Kuanchertchoo, N. Wetprasit and P. Supaphol, *Materials Science and Engineering: C*, 2012, **32,** 758-762.

21. B.D. Ulery, L.S. Nair and C.T. Laurencin, *Journal of Polymer Science Part B: Polymer Physics*, 2011, **49,** 832-864.

22. Q.L. Loh, Y.Y. Wong and C. Choong, *Colloid and Polymer Science*, 2012, **290,** 619-629.

23. Y.Y. Wong, S. Yuan and C. Choong, *Polymer Degradation and Stability*, 2011, **96,** 2189-2197.

24. F. He, B. Luo, S. Yuan, B. Liang, C. Choong and S.O. Pehkonen, *RSC Adv.*, 2014, **4**, 105-117.

25. L.E. Flynn, *Biomaterials*, 2010, **31,** 4715-4724.

26. J. Liao, E.M. Joyce and M.S. Sacks, *Biomaterials*, 2008, **29,** 1065-1074.

27. B.N. Brown, J.M. Freund, L. Han, J.P. Rubin, J.E. Reing, E.M. Jeffries, M.T. Wolf, S. Tottey, C.A. Barnes, B.D. Ratner and S.F. Badylak, *Tissue Engineering Part C, Methods*, 2011, **17,** 411-421.

28. A. Barth, *Biochim. Biophys. Acta.*, 2007, **1767,** 1073-1101.

29. H.Y. Hu and H.N. Du, *J. Protein Chem.*, 2000, **19,** 177-183.

30. J. Grdadolnik and Y. Maréchal, *Biopolymers*, 2001, **62,** 40-53.

31. K. Gelse, E. Pöschl and T. Aigner, *Adv. Drug Deliv. Rev.*, 2003, **55,** 1531-1546.

32. Q.L. Loh and C. Choong, *Tissue Engineering Part B, Reviews*, 2013 **19,** 485-502.

33. O. Guillaume, A. Daly, K. Lennon, J. Gansau, S.F. Buckley and C.T. Buckley, *Acta Biomater*., 2014, **10,** 1985-1995.

34. L. Elowsson, H. Kirsebom, V. Carmignac, M. Durbeej and B. Mattiasson, *J. Mater. Sci. Mater. Med.*, 2012, **23,** 2489-2498.

FIGURE CAPTIONS

Fig. 1 Schematic illustration of the various steps involved in the (a) fabrication and (b) surface modification of the porous OVA microcarriers.

Fig. 2 The effectiveness of the chemical-free decellularization method and the preservation of ECM components after decellularization was confirmed by (a) H&E staining, showing the absence of nuclei material, (b) SEM analysis showing the absence of lipids and cells within the fibrous LpECM material, (c) change in color of the final freeze-dried LpECM upon removal of lipids, and (d-f) positive immunostaining for collagen I, collagen IV and laminin respectively.

Fig. 3 FTIR spectra of the (a) raw OVA powder, (b) OVA microcarrier and (c) OVA-LpECM hybrid microcarriers. Successful crosslinking and surface modification during the fabrication process was confirmed by the presence of characteristic peaks (red dotted boxes).

Fig. 4 Schematic illustration of the BDE-crosslinking mechanism under acidic conditions used in the fabrication of the OVA microcarriers. During this process, the epoxide groups of BDE bond (circled) with the carboxyl groups of the collagen to form carboxylate ester groups.

Fig. 5 Morphology of the OVA microcarriers: (a) Image of the pure OVA microcarrier after freeze drying, (b-d) SEM images of OVA microcarriers with OVA : alginate ratios

2:1, 1:1 and 1:2 respectively, (e) image of the OVA-LpECM microcarrier, (f-h) cross-sectional SEM images of OVA-LpECM microcarriers with OVA-alginate ratios 2:1, 1:1 and 1:2 respectively and (i) the size distribution of one hundred OVA and OVA-LpECM microcarriers (n=100). The different amounts of alginate used in the fabrication process results in different pore architectures and porosity, and both OVA and OVA-LpECM microcarriers have interconnected pores.

Fig. 6 Mechanical testing results for the OVA and OVA-LpECM microcarriers of different OVA : alginate ratios under compression. OVA-LpECM microcarriers had significantly better (*p<0.05) mechanical strength than pure OVA microcarriers with the same corresponding OVA to alginate ratio. With decreasing OVA to alginate ratio, an increase in compressive moduli was observed for both OVA and OVA-LpECM microcarriers.

Fig. 7 Graph showing the swelling behavior of OVA and OVA-LpECM microcarriers. Increasing alginate to OVA ratios, led to significantly higher (*p<0.05) swelling ratios for both OVA and OVA-LpECM microcarriers.

Fig. 8 Cellular results for OVA and OVA-LpECM microcarriers, (a) the addition of LpECM material to the OVA microcarriers significantly improved (*p<0.05) cellular attachment and proliferation, and (b-e) LIVE/DEAD® staining after 1 day and 7 days of *in vitro* culture on (b,d) OVA microcarriers and (c,e) OVA-LpECM microcarriers respectively.

Table 1. Comparison of the porosities, pore size ranges and mean pore sizes of OVA and OVA-LpECM scaffolds

Samples	Ratio (OVA : Alginate)	Porosity (%)	Pore size range (μm)	Mean pore size (μm)
OVA	2:1	33.68±5.52	27.92-163.49	116.48±38.36
	1:1	41.73±4.96	26.39-159.22	120.72±43.58
	1:2	57.40±3.51	29.13-178.36	138.48±39.17
OVA-LpECM	2:1	30.36±3.26	23.42-186.57	121.27±37.74
	1:1	37.89±4.35	25.67-175.73	129.53±40.08
	1:2	49.28±2.05	31.72-196.95	139.05±42.72

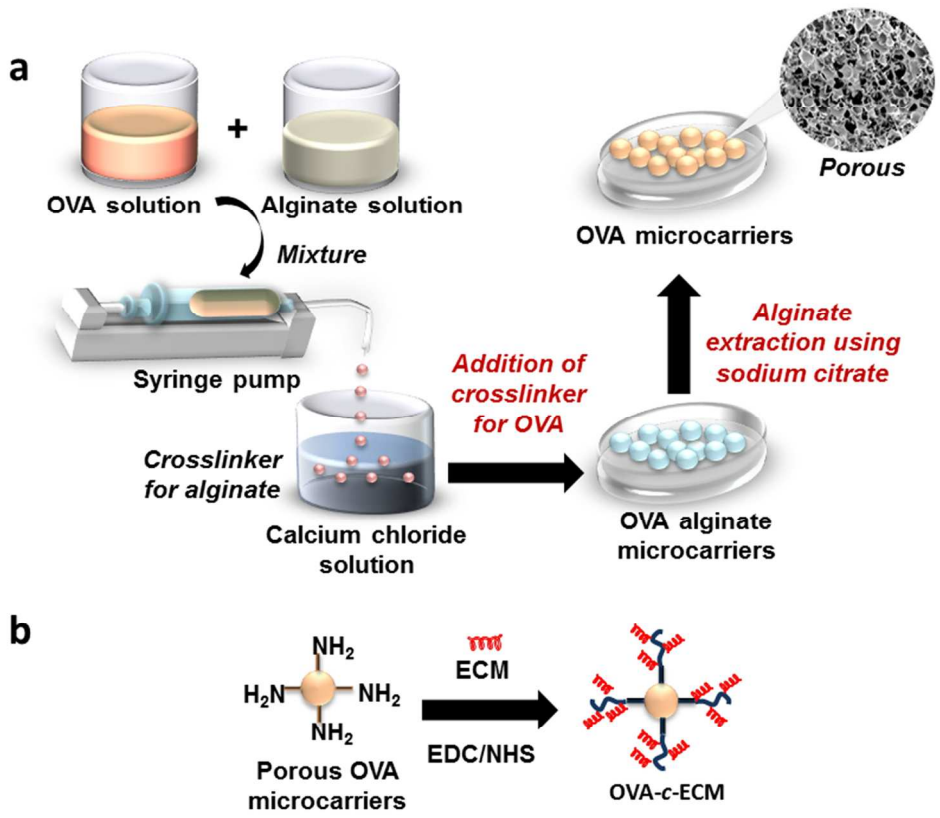

Fig. 1 Schematic illustration of the various steps involved in the (a) fabrication and (b) surface modification of the porous OVA microcarriers.
189x156mm (300 x 300 DPI)

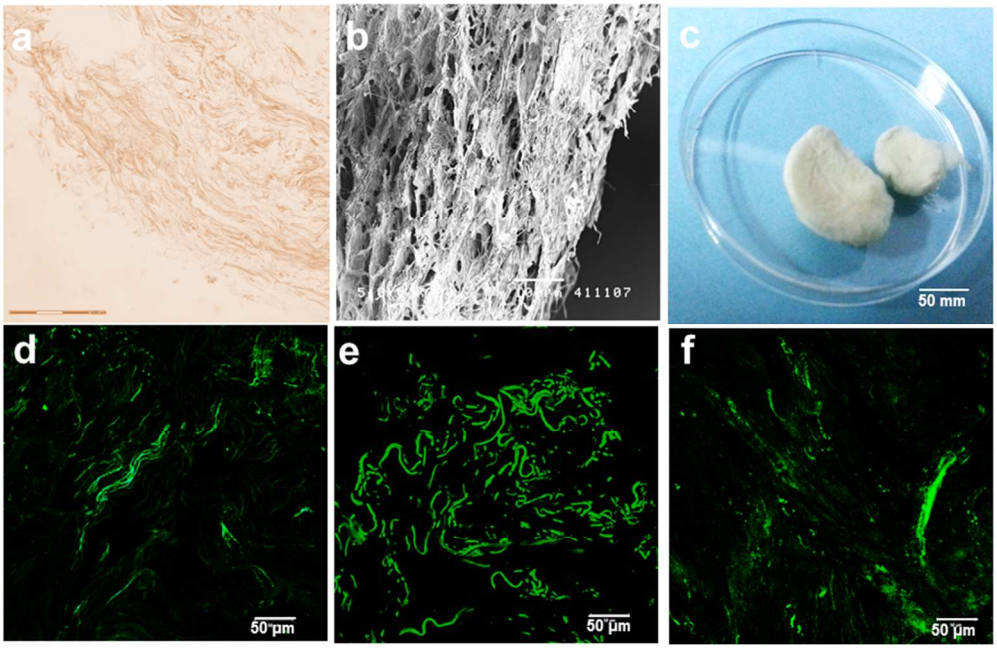

Fig. 2 The effectiveness of the chemical-free decellularization method and the preservation of ECM components after decellularization was confirmed by (a) H&E staining, showing the absence of nuclei material, (b) SEM analysis showing the absence of lipids and cells within the fibrous LpECM material, (c) change in color of the final freeze-dried LpECM upon removal of lipids, and (d-f) positive immunostaining for collagen I, collagen IV and laminin respectively.
189x121mm (300 x 300 DPI)

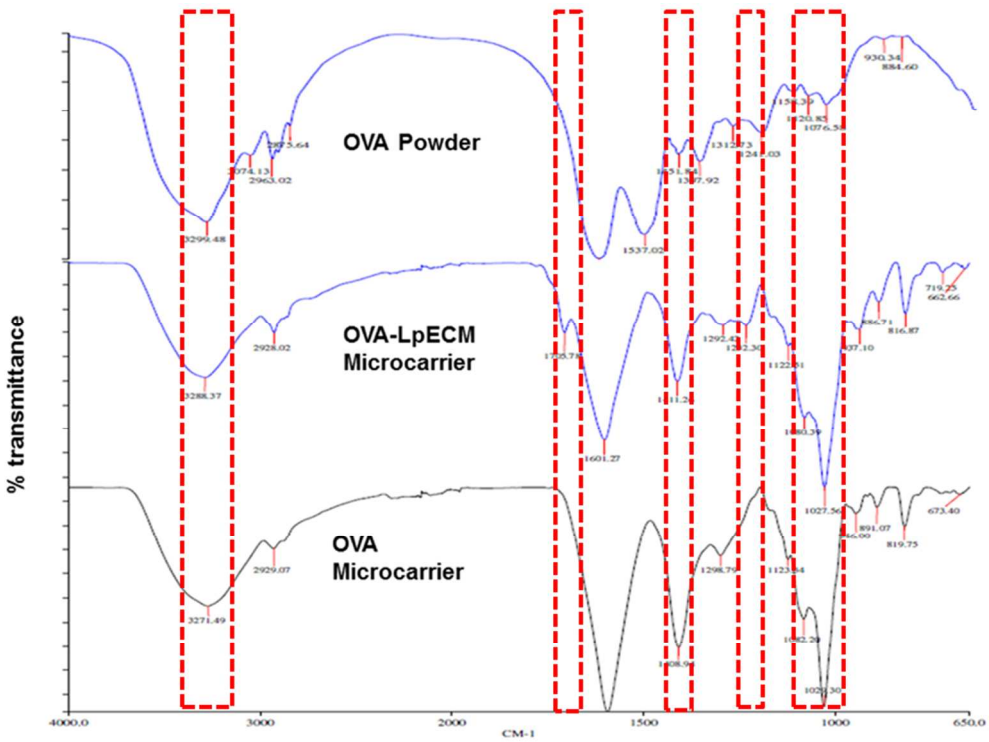

Fig. 3 FTIR spectra of the (a) raw OVA powder, (b) OVA microcarrier and (c) OVA-LpECM hybrid microcarriers. Successful crosslinking and surface modification during the fabrication process was confirmed by the presence of characteristic peaks (red dotted boxes).
249x185mm (300 x 300 DPI)

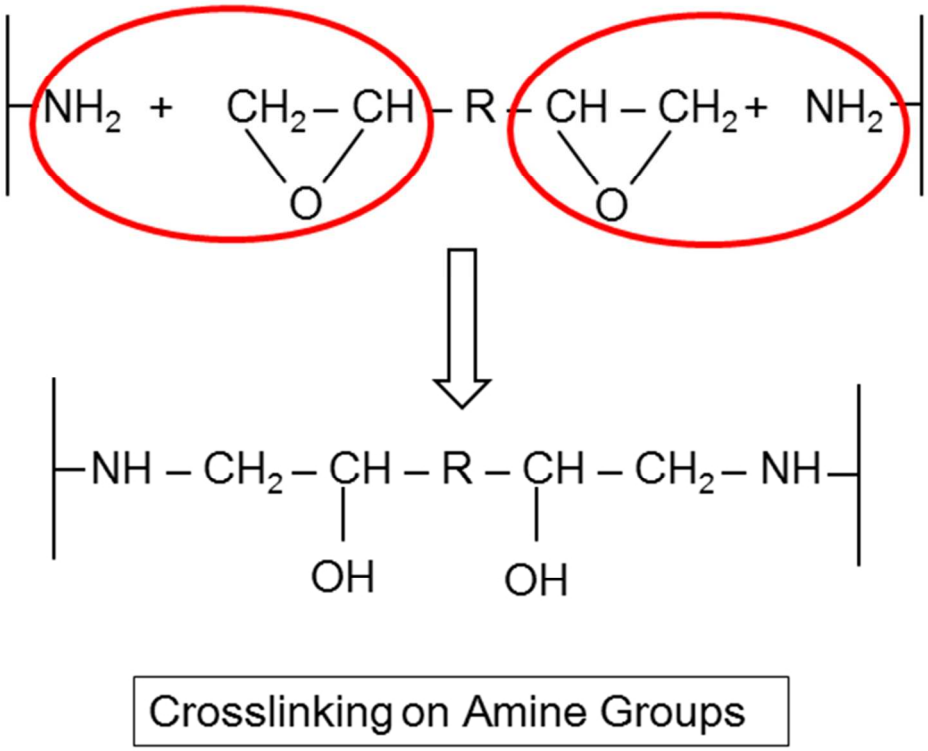

Fig. 4 Schematic illustration of the BDE-crosslinking mechanism under acidic conditions used in the fabrication of the OVA microcarriers. During this process, the epoxide groups of BDE bond (circled) with the carboxyl groups of the collagen to form carboxylate ester groups.
90x72mm (300 x 300 DPI)

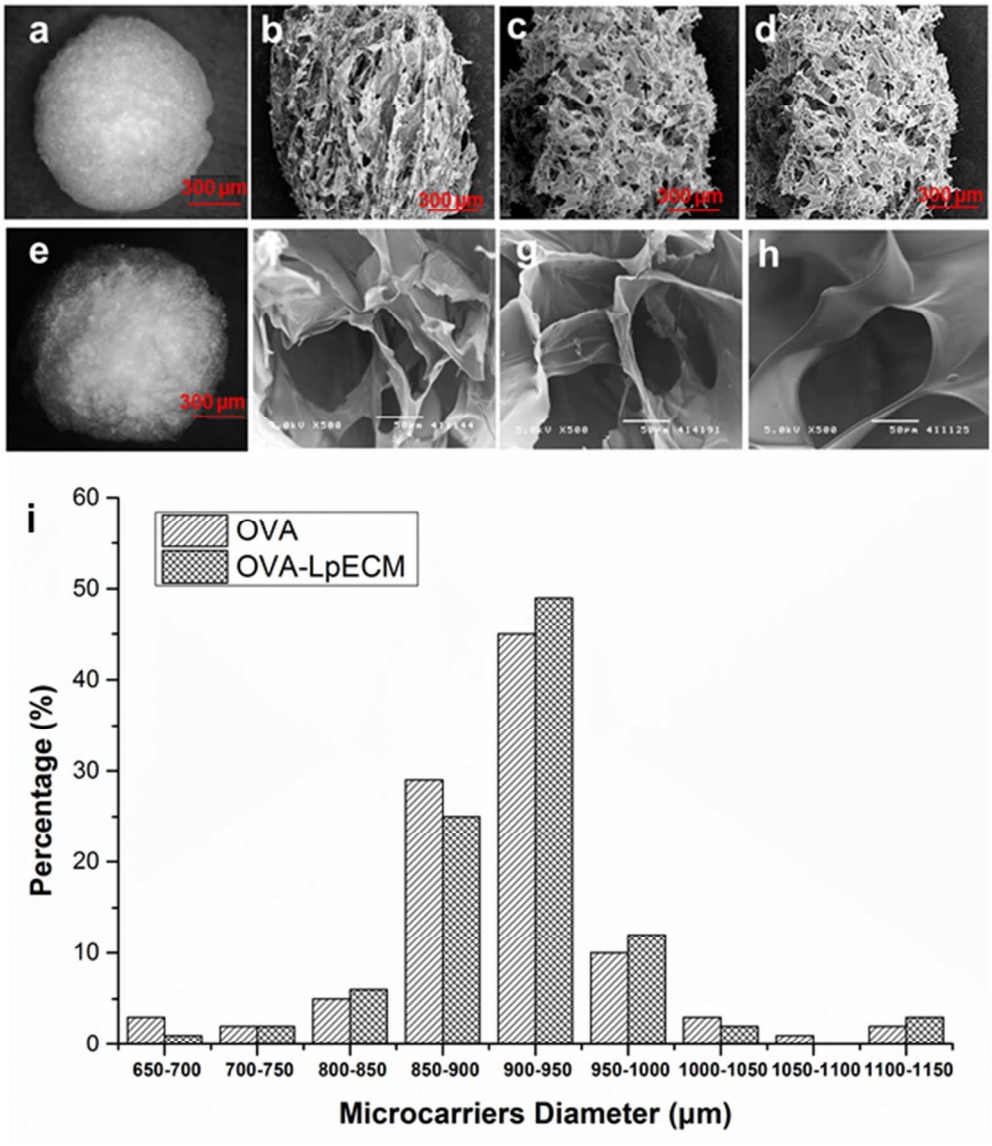

Fig. 5 Morphology of the OVA microcarriers: (a) Image of the pure OVA microcarrier after freeze drying, (b-d) SEM images of OVA microcarriers with OVA : alginate ratios 2:1, 1:1 and 1:2 respectively, (e) image of the OVA-LpECM microcarrier, (f-h) cross-sectional SEM images of OVA-LpECM microcarriers with OVA-alginate ratios 2:1, 1:1 and 1:2 respectively and (i) the size distribution of one hundred OVA and OVA-LpECM microcarriers (n=100). The different amounts of alginate used in the fabrication process results in different pore architectures and porosity, and both OVA and OVA-LpECM microcarriers have interconnected pores.
166x190mm (300 x 300 DPI)

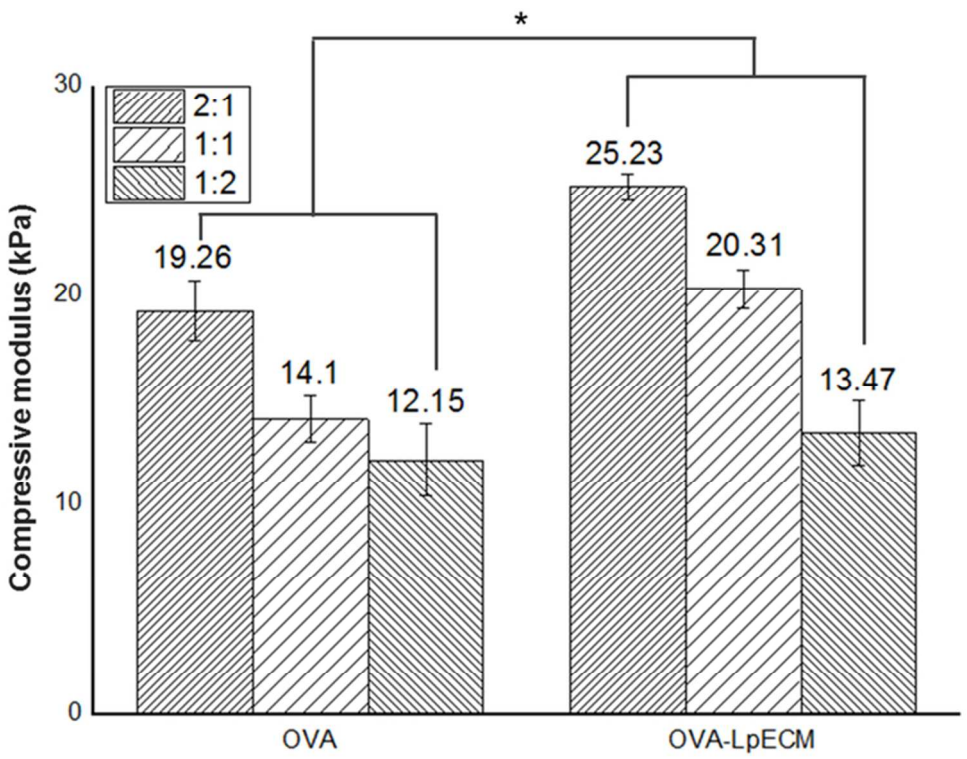

Fig. 6 Mechanical testing results for the OVA and OVA-LpECM microcarriers of different OVA : alginate ratios under compression. OVA-LpECM microcarriers had significantly better (*p<0.05) mechanical strength than pure OVA microcarriers with the same corresponding OVA to alginate ratio. With decreasing OVA to alginate ratio, an increase in compressive moduli was observed for both OVA and OVA-LpECM microcarriers.
68x52mm (300 x 300 DPI)

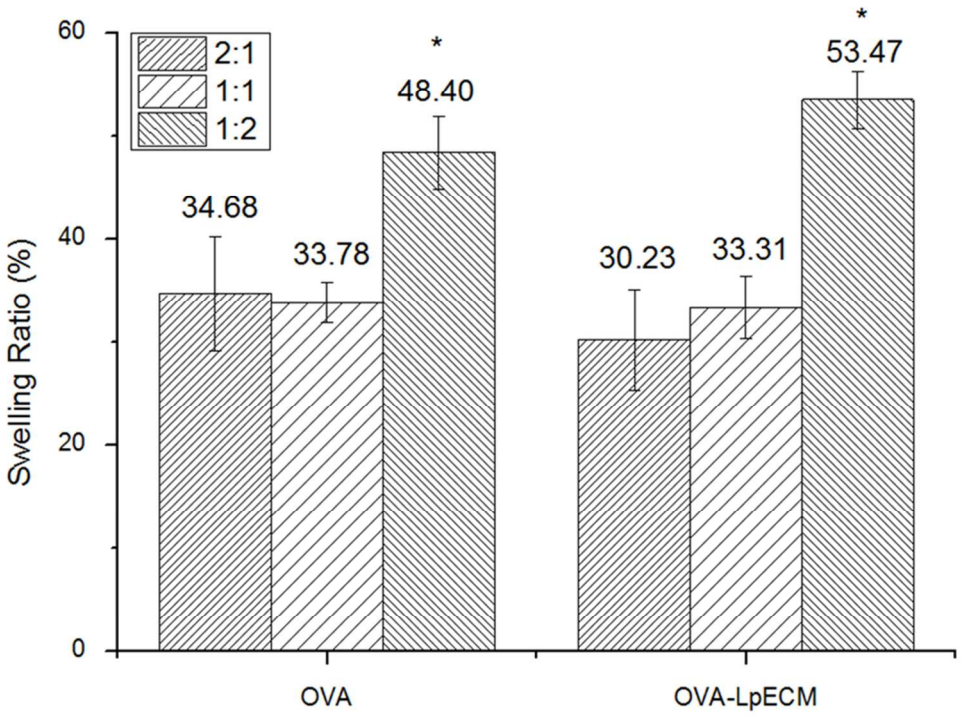

Fig. 7 Graph showing the swelling behavior of OVA and OVA-LpECM microcarriers. Increasing alginate to OVA ratios, led to significantly higher (*p<0.05) swelling ratios for both OVA and OVA-LpECM microcarriers.
139x102mm (300 x 300 DPI)

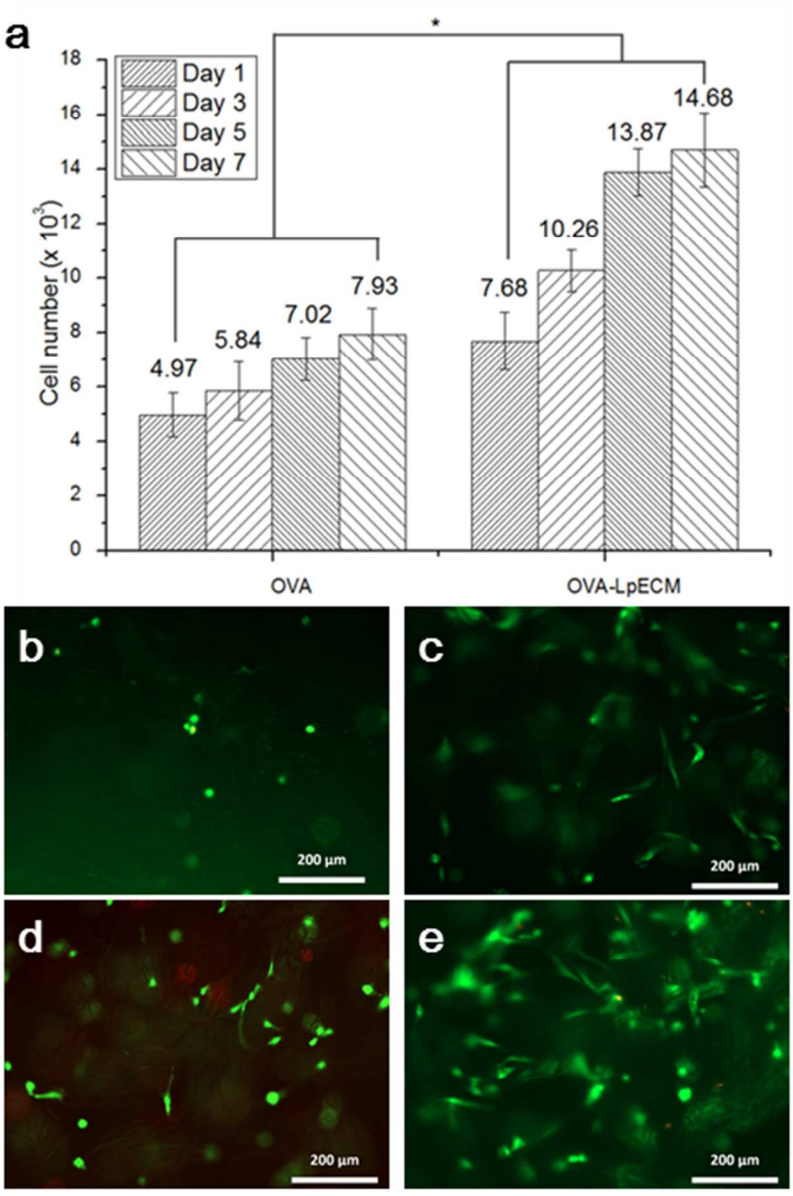

Fig. 8 Cellular results for OVA and OVA-LpECM microcarriers, (a) the addition of LpECM material to the OVA microcarriers significantly improved (*p<0.05) cellular attachment and proliferation, and (b-e) LIVE/DEAD® staining after 1 day and 7 days of in vitro culture on (b,d) OVA microcarriers and (c,e) OVA-LpECM microcarriers respectively.
132x190mm (300 x 300 DPI)